Time-resolved x-ray-scattering study of ordering kinetics in bulk single-crystal Cu_3Au

Robert F. Shannon, Jr., Stephen E. Nagler, and Curt R. Harkless
University of Florida, Gainesville, Florida 32611

Robert M. Nicklow
Oak Ridge National Laboratory, Oak Ridge, Tennessee 37831

(Received 12 August 1991; revised manuscript received 2 January 1992)

Time-resolved x-ray scattering has been used to study ordering kinetics in single-crystal bulk Cu_3Au. After annealing at high temperatures, the sample is rapidly quenched to fixed temperatures below the order-disorder transition temperature. The development of order is monitored in real time with use of scattering techniques. The data clearly showed three regimes: nucleation, ordering, and coarsening. The anisotropic superlattice peaks that reflect the domains structure are investigated in connection with the ordering kinetics. The line shape of the scattering function exhibits a crossover from a Gaussian to a Lorentzian squared as the system goes from the ordering regime to the coarsening regime. The line shape of $S(Q)$ is analyzed by fitting the data with a variety of functions. The resolution is accounted for during the fitting. The coarsening in Cu_3Au is consistent with curvature-driven growth.

I. INTRODUCTION

The ordering kinetics of first-order phase transitions have been of great interest in the past decade.[1-6] Theoretical,[1,2,7-23] experimental,[24-41] and computer simulation[3,23,42-61] studies on first-order phase transitions abound. The phenomena have been studied in a variety of systems, including binary alloys binary fluids, magnetic materials, block copolymers, glasses, ferroelectric crystals, and others.[14] A focus of interest has been the nonequilibrium scaling and apparent universality in late-stage growth kinetics.[6] Conservation laws are the most important factor in determining the behavior of late-stage kinetics. The effects of symmetry, structure of domain walls, impurities, and stoichiometry may also be important but are not as well understood.

The general problem is often discussed in terms of the Ising model,[62] for which the order parameter is simple enough for the system to be easily classified. For example, the ferromagnet with spin-exchange (Kawasaki)[3] dynamics has a conserved order parameter (COP). On the other hand, ferromagnets with spin-flip (Glauber)[63] dynamics have a nonconserved order parameter (NCOP). For antiferromagnets, the appropriate order parameter is the sublattice magnetization, which is a nonconserved quantity for either Glauber or Kawasaki dynamics.[12]

In this article we present the results of a time-resolved x-ray-scattering study of the ordering kinetics in a prototypical system with an order-disorder transition: the binary alloy Cu_3Au. The order-disorder transition in Cu_3Au is analogous to the antiferromagnet with Kawasaki dynamics for which the net magnetization is conserved. In the alloy the equivalent conserved quantity is the concentration. However, the order parameter is not conserved.

The subject of interest is the formation of an ordered state in a system that is initially disordered, then rapidly quenched into a region of the phase diagram where the equilibrium state is ordered. For the order-disorder transition we discuss, the quench is implemented by a rapid change of temperature from an initial temperature T_i to a final temperature T_f, where the equilibrium transition temperature is T_c, and $T_f < T_c < T_i$.

Immediately after the quench, the system is in the disordered state characterized by the high-temperature phase. A fluctuation into the low-temperature equilibrium state is necessary to begin the formation of ordered regions. In a mean-field picture the disordered state can be classified as either metastable or unstable.[64] For metastable states, ordering is initiated via nucleation (a localized fluctuation), while for unstable states the fluctuations are delocalized, leading to spinodal decomposition. In a real system the distinction between metastable and unstable regimes is not well defined, nevertheless the concepts retain some validity as a limiting behavior.

For shallow quenches ($\Delta T \equiv T_c - T_f \ll T_c$) order-disorder transitions usually lead to behavior consistent with a nucleation picture.[65] There is some experimental evidence that for sufficiently deep quenches spinodal ordering produces a better description.[65-68]

Following nucleation, the ordered regimes grow into the disordered matrix. This process may be called the growth of order or ordering. Eventually the domain walls will meet. If the ground state is degenerate, the resulting structure will be an interpenetrating array of domain walls separating regions ordered in the different ground states. The domain walls contain excess free energy which the system reduces by growing larger domains. The evolution to larger domains is called coarsening (or Ostwald ripening).

In the coarsening regime the average domain size at time t after the quench is described by a single length $L(t)$. At different times the domain structure looks the same when lengths are measured in units of $L(t)$. The system is in this sense self-similar under a rescaling of both length and time. Figure 1 illustrates this self-

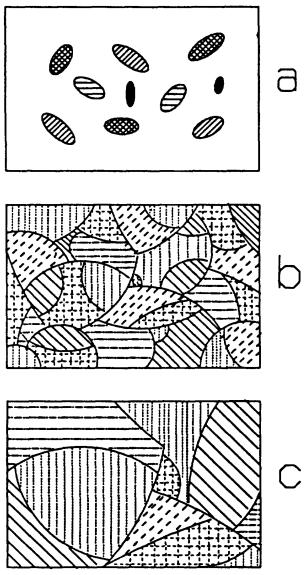

FIG. 1. Growth of order and coarsening after a quench. (a) Growth of order shortly after the onset of critical nucleation, (b) Early state of domain coarsening, (c) Late stage of domain coarsening.

similarity. The consequences of this nonequilibrium scaling are particularly evident in the structure factor for the system. If the order parameter is denoted as Ψ the nonequilibrium structure factor $S(\mathbf{Q},t)$ can be written as

$$S(\mathbf{Q},t) \propto \int \langle \Psi(0,t)\Psi(\mathbf{r},t)\rangle e^{i\mathbf{Q}\cdot\mathbf{r}} d^3r \ . \tag{1}$$

In the scaling regime one finds

$$S(\mathbf{Q},t)=[L(t)]^d \tilde{S}_{\hat{\mathbf{e}}}(\mathbf{q}L(t)) \ , \tag{2}$$

where d is the dimension of the system, $\mathbf{q}=\mathbf{Q}-\mathbf{G}$ where $\mathbf{G}$ is a wave vector characterizing the ordered structure, and $\hat{\mathbf{e}}=\mathbf{q}/q$ is a unit vector denoting the fact that $\tilde{S}$ is in general anisotropic.

$S(\mathbf{Q},t)$ is directly measured by x-ray-scattering techniques when the order parameter is linearly related to the charge density. The *nonequilibrium* $S(\mathbf{Q},t)$ discussed here should not be confused with the frequency-domain Fourier transform of the *equilibrium* dynamic structure factor $S(\mathbf{Q},\Omega)$.[69]

The actual form of $\tilde{S}(\mathbf{Q}L)$ is a subject of recent interest. The general form depends on whether or not Ψ is conserved. For systems with a COP, $S(\mathbf{Q},t)$ has a fixed value at $\mathbf{Q}=0$, and a peak at some $\mathbf{Q}_{\max}$. The domain size $L \sim Q_{\max}^{-1}$, or some similar measure such as the first moment of $S(\mathbf{Q},t)$. Conversely, for NCOP systems, $S(\mathbf{Q},t)$ is peaked at the ordering wave vector(s) $\mathbf{G}$. The domain size $L(t)$ is inversely proportional to the full width at half maximum (FWHM) of $S(\mathbf{q},t)$. The precise functional form as well as anisotropy are important theoretically and experimentally. These issues are discussed in more detail below.

Beyond the form of $S(\mathbf{Q},t)$, scaling is also manifested in the growth rate of the domains. In a pure system at late times one expects

$$L(t)=t^a \ . \tag{3}$$

The usual situation is, for NCOP $a=\frac{1}{2}$ (curvature-driven growth),[16] while for COP $a=\frac{1}{3}$ (Lifshitz-Slyozov growth).[15] These behaviors are consistent with the results of experiment,[24–41,70] simulations,[42–61,71] and theory.[7–23,72–75] Other situations can arise, in particular if randomness is present, then the domain size may grow logarithmically.[76–82] The form of $L(t)$ provides an important experimental distinction between classes of ordering systems.

A recent proposal[14] divides growth kinetics into four classes characterized by different low-temperature behaviors. Class 1 systems are analogous to a simple Ising ferromagnet with Glauber dynamics. Class 1 systems obey power-law domain growth at all temperatures. Class 2 differs from class 1 only in that members have local defects that cause freezing of the domain growth at absolute zero. These local defects have activation energies that are independent of domain size L. Pure alloys such as Cu_3Au are probable members of this second classification. Classes 3 and 4, on the other hand, have defects with $L(t)$-dependent activation energies, leading to logarithmic growth. Type 3 and 4 systems are differentiated by the power m of the logarithmic growth of the form $L \sim \ln(t)^m$. Class 3 has $m=1$, and is likely to contain the random-field Ising model. Class 4 has $m \neq 1$, and may include dilute ferromagnets and spin glasses.

This paper focuses on a careful study of the ordering kinetics in the alloy Cu_3Au. Cu_3Au is a prototypical system with a first-order transition, a fourfold degenerate ground state, and a nonconserved order parameter (NCOP). As discussed below, there is also an interesting, nontrivial anisotropy.[83–85]

At high temperatures Cu_3Au has a face-centered-cubic (fcc) lattice where each site is randomly occupied by either a Cu (probability 0.75) or a Au (probability 0.25) atom. Below the critical ordering temperature $T_c \sim 390$ °C the system develops an ordered structure as shown in Fig. 2. The Au atoms occupy the corners of a conventional cubic unit cell while the Cu atoms sit at the face centers. Since the "corner" can be chosen in four ways the ground state is fourfold degenerate.

Two distinct types of domain walls separate regions in each of the four ground states. The first of these walls conserves the nearest-neighbor configurations and is easily formed due to its low energy.[86] We denote the cubic axis by $\{a_i\}$. Type-1 walls can be formed by displacing the atoms on one side of a plane perpendicular to the a_3 axis by $(a_1+a_2)/2$ as in Fig. 3. This is true for cyclic permutations of (a_1,a_2,a_3). Type-1 walls are often called "half-diagonal glide" walls. A type-2 wall can be formed by displacing the atoms on one side of a plane perpendicular to a_3 by $(a_1+a_3)/2$, as in Fig. 4. The important difference between the walls is that type-1 walls conserve the nearest-neighbor configuration where type-2 walls do not. Type-2 walls therefore have a higher surface energy.[84] In addition to the raised surface energy, it is interesting to note that the composition of the lattice in the vicinity of a type-2 wall has the wrong stoichiometry: A type-2 wall results in a region with 100% Cu or a region

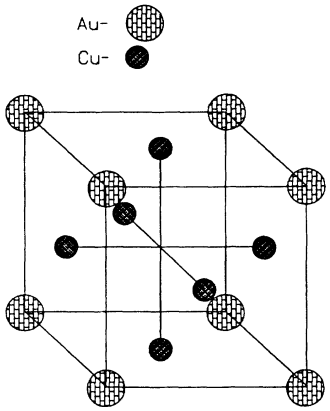

FIG. 2. Schematic of fcc structure for ordered Cu_3Au.

with 50% Cu and 50% Au atoms. This suggest, in a very naive picture, that significant diffusion might have to take place to move a type-2 wall. One could speculate that purely diffusional wall motion would lead to a growth exponent of a $a=\frac{1}{3}$, rather than $a=\frac{1}{2}$ as expected for the NCOP situation in Cu_3Au. As shown below, the coarsening of type-2 walls is indeed consistent with curvature-driven growth as expected for a system with a NCOP.

If all domain walls separating ordered ground states were indistinguishable, the Cu_3Au system would be equivalent to the four-state Potts model on a three-dimensional simple cubic lattice. By symmetry, the transition in this model is always first order.[87] This correspondence is not exact, however, this does not affect the order of the transition.[88]

The coarse-grained Ginzburg-Landau Hamiltonian appropriate for Cu_3Au has been derived by Lai.[88] The order parameter has three components[88,89] and there is a conservation law for atomic concentrations. The Hamiltonian is distinguished from that of the four-state Potts model by the presence of an anisotropy term arising from the domain-wall structure.

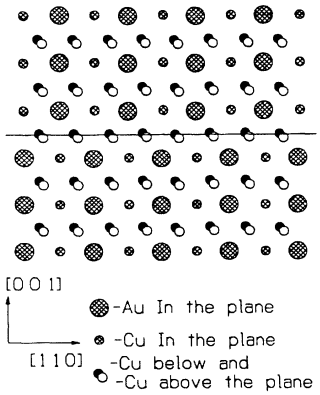

FIG. 3. Domains of different phase separated by a type-1 domain wall as described in the text. The line marks the position of the wall.

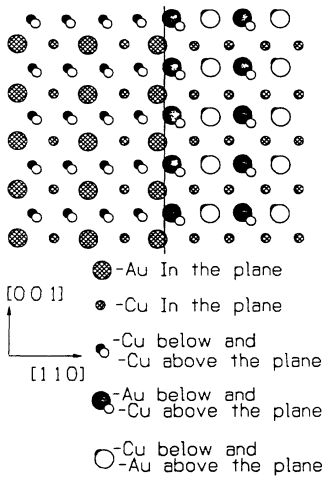

FIG. 4. Domains of different phase separated by a type-2 domain wall as described in the text.

The order parameter Ψ is linear in the atomic concentrations, so scattering experiments probe $S(\mathbf{Q})$ or $S(\mathbf{Q},t)$. The low-temperature structure is simple cubic, so that superlattice peaks corresponding to ordering wave vectors appear at reciprocal lattice points that have vanishing structure factors for an fcc crystal viewed as a cubic lattice with a basis. The existence of a domain structure causes the scattering from superlattice peaks to be anisotropic in reciprocal space. The peaks are disk shaped, with the radius determined primarily by the density of type-1 walls, and with the thickness arising primarily from the density of type-2 walls. Figure 5 shows the orientations of the disk of scattering at superlattice points.

There have been many studies of the ordering kinetics in Cu_3Au.[83,90] Notable early work included measurements of the resistivity as a function of time following a temperature quench.[90] The resistance evolved from the high-temperature value to a much lower value in the ordered state, and the fraction of ordered material was assumed to be linear in the change of resistivity. Several different regimes were observed. Modern work has emphasized scattering techniques.[27,66,70,91] The present x-ray-scattering study examines the different regimes for

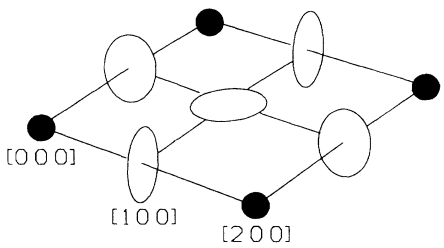

FIG. 5. Shapes of the reflections in reciprocal space for type-1 walls normal to the three axes. The fundamental reflections are spheres, and the superlattice reflections are disk shaped.

ordering and the form of the nonequilibrium scaling in an anisotropic system. Some preliminary results have been previously published.[91]

The rest of this paper is arranged as follows: Section II describes the experimental techniques employed. The analysis of the data is presented in Sec. III. A discussion of the results is contained in Sec. IV, and the summary and conclusions comprise Sec. V.

II. EXPERIMENTAL DETAILS

The crystalline sample of Cu_3Au used in these experiments was cut at Oak Ridge National Laboratories to expose the $(h,0,0)$ face. In order to remove any oxidation the surface was etched in nitric acid and then annealed for 12 h at 700 °C under an Ar atmosphere.

The sample was mounted on a Ti-backed Cu plate attached directly to a resistively heated Cu post. Temperature was measured by a K thermocouple held directly on the face of the sample. A second K thermocouple used for control measured the temperature at the connection between the Cu plate and heated post. A crude estimate of the expected temperature gradient was made using the thermal conductivity of Cu and Au and the Stefan-Boltzmann law, weighted by the emissivity of Cu and Au. The estimate assumed that the crystal was heated at one end only, the result yielded a linear gradient of 0.01 °C/mm. The x-ray spot size on the sample was roughly 1×6 mm^2, consequently the temperature difference within the area measured by x-rays should be no more than 0.06 °C. The temperature control was good to ±0.3 °C over several hours and ±0.5 °C over several days. Therefore, the gradient was negligible relative to the temperature stability.

The crystal was placed in an evacuated furnace equipped with Be windows for x-ray work. The quenches were arranged so that the temperature went smoothly to the final value. Quenches were performed by shutting off power to the heater. The zero of time was denoted by the point at which the temperature (initially high) crossed the measured transition temperature. If the time for completion of a quench represented here is defined by the final temperature being stable within 1 °C, the quenches were completed within 30–90 sec, depending on the quench depth. For subsequent work,[91,92] the furnace incorporated a quenching loop, which cut quenching times drastically. For the intermediate to late stages under discussion in this paper the quench rate is insignificant.

The furnace was mounted so that the sample surface was at the center of rotation of a four-circle x-ray diffractometer. The scattering plane used in most of the measurements was the $(hk0)$ plane, which allowed for careful study of the fundamental and superlattice peaks in the $[0k0]$ direction. The x-rays were generated by an 18-kW rotating anode with a Cu target. As discussed below, it was necessary to employ several different geometries to fully characterize the sample in the time-resolved experiments.

Most of the initial characterization measurements employed a standard double-crystal four-circle diffractometer, as illustrated in Fig. 6(a). The Cu $K\alpha$ x rays coming from a point source were reflected off a flat monochromator to the sample through collimating slits and an evacuated beam path. A thin Mylar sheet scattered a small fraction of the incident beam into a vertically mounted Bicron scintillation counter serving as a monitor, allowing the data to be normalized to the incident intensity. The beam scattered from the sample was then Bragg reflected by an analyzer crystal into a second Bicron detector. The spot size of the beam at the sample position was 1×6 mm^2. Some subsequent time-resolved measurements utilized a vertical line geometry x-ray source and a Braun Pt wire-based proportional-counter position-sensitive detector (PSD) [see Fig. 6(b)].

The structural perfection of the sample was investigated using standard double-crystal techniques with a Si(111) monochromator and analyzer. For example, the mosaic spread measured at the (020) peak is shown in Fig. 7. The FWHM of the mosaic spread is 0.25°. The equilibrium temperature dependence of the scattering was measured using double-crystal methods with a pyrolitic graphite (PG) (002) monochromator and analyzer.

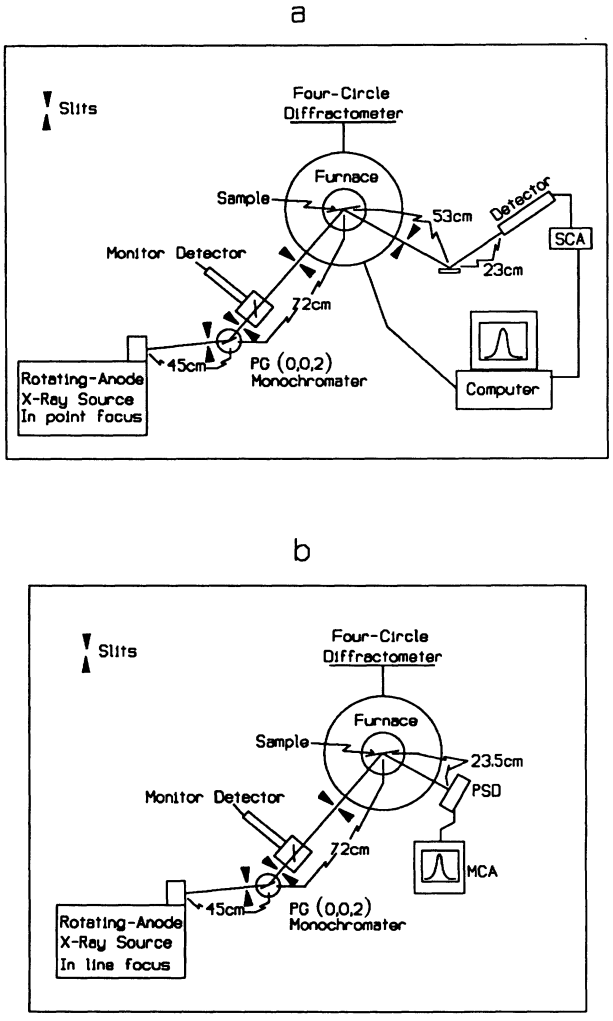

FIG. 6. Layout of equipment: (a) Transverse setup, (b) radial setup.

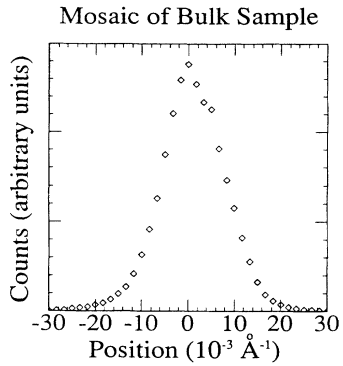

FIG. 7. High-resolution mosaic spread scan at the (020) of Cu_3Au.

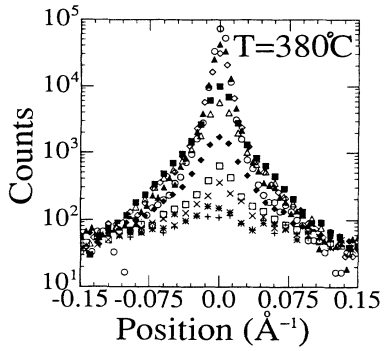

FIG. 8. Ten of 350 raw transverse scans from a quench to 380.5 °C. The times in minutes after the quench for each scan in order of increasing amplitude are 2.5, 7.6, 22.7, 32.8, 52.9, 87.8, 122.7, 336.9, 501.5, and 1706.3. A plot of transverse scans on a linear scale can be found later in the text. Some of the points in the tails of the scans are outside of the range plotted.

In order to determine the transition temperature the intensity of the (010) peak was recorded as a function of time for several temperatures after raising the temperature from below T_c to near T_c. At 385.2 °C the peak was observed for 3.5 h and an extrapolation suggested that the sample would almost disorder but not completely. On the other hand, at 385.7 °C the peak was nearly gone after 1.5 h clearly showing that the sample was above T_c. The transition temperature was then taken to be the value of a weighted average based on extrapolations of the rate of decay of the peak, and found to be 385.3 °C. This extrapolation is not very important because the temperatures used are only half a degree apart, but it was clear that the transition was closer to 385.2±0.5 than 385.7±0.5 °C. This operational definition of T_c is within the range of transition temperatures reported in the literature of $T_c = 388 \pm 3$ °C.[83,93]

In the temperature region where the determination of T_c was made, the cubic lattice constant of the sample was measured as $a = 3.771$ Å, consistent with values reported in the literature.[94] The precise values of T_c and lattice constant reported in the literature are somewhat sample dependent,[93,94] but each has a clear dependence on stoichiometry. Accepting the mean literature values, the measured lattice constant rules out an excess concentration of Au atoms of more than 0.6%. The transition temperature rules out an excess concentration of Cu atoms of more than 0.4%, so the stoichiometry is known to be Cu_xAu_{1-x}, where $0.744 \leq x \leq 0.754$. The outer bounds here are conservative estimates, and the portion of the sample being measured with x rays is operationally stoichiometric.

The time-resolved measurements concentrated on the (010) superlattice peak. In order to account for the anisotropy in the scattering at the (010) it was necessary to employ two different setups. Scans about the (010) peak in the $[h00]$ direction (referred to below as transverse scans) were carried out with a double-crystal setup using a pyrolytic graphite (002) monochromator and analyzer [Fig. 6(a)]. The instrumental resolution was measured directly by placing a perfect Ge (111) crystal at the sample position and measuring the (111) reflection. The intrinsic width of a Ge single-crystal peak is negligible compared to the instrumental resolution. Since the Bragg angle 2θ for Ge (111) using Cu $K\alpha$ radiation is 27.2° and that for Cu_3Au (010) is 23.6°, the geometric correction to the resolution function is negligible. The HWHM of the resolution function in the $[h00]$ direction is 0.003 Å^{-1}, in the $[0k0]$ direction it is 0.01 Å^{-1}, and in the [001] direction it is greater than 0.1 Å^{-1}. This setup was suitable for obtaining detailed measurements in the transverse $[h00]$ direction. The measured resolution function is consistent with known theoretical treatments of the resolution.[95,96]

To improve the resolution for scans along the $[0k0]$ direction (radial scans) a second setup employed a line geometry source and a position-sensitive detector [Fig. 6(b)]. The PSD data represents a scan in the angle 2θ rather than a true radial scan, but for small ranges of 2θ they are essentially equivalent. The resolution depends on the sample-to-detector distance. For the sample-to-detector distance used (23.5 cm) each channel of the PSD corresponds to 0.0125° in 2θ. The window on the PSD was 5 cm long, which corresponds to a solid angle of 10.3°.

For the radial setup over 90% of the $K\alpha_2$ ($\lambda = 1.544\,33$ Å) intensity was slit out leaving mostly $K\alpha_1$ ($\lambda = 1.540\,51$ Å) where the subscripts define the two components of the doublet line. For the Cu_3Au experiment the slitting out of $K\alpha_2$ was done on the (020) peak with the presample slits shown in Fig. 6(b). At the (020), $K\alpha_1$ and $K\alpha_2$ were well separated, as opposed to at the (010) where the two components were not completely resolved. It was important to slit out $K\alpha_2$ due to the complications it would have added to the resolution correction. In the transverse setup it was not necessary to do so because of the analyzer. The resulting instrumental resolution was 0.003 Å^{-1} (HWHM).

Typical examples of the raw data from the (010) peak obtained in the quenches are presented in Figs. 8 and 9. Figure 8 contains transverse scans and Fig. 9 contains radial scans. Initially the peaks are broad with a small amplitude. As time passes they grow in amplitude and be-

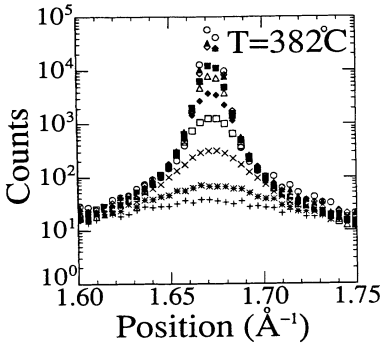

FIG. 9. Ten of 207 radial scans from a quench to 382 °C. The times in minutes after the quench for each scan in order of increasing amplitude are 2.5, 7.6, 22.1, 32.2, 52.5, 87.9, 128.5, 346.2, 500.7, and 2668.4. Only the central portion of each scan is shown and the data has been binned in groups of five for clarity of presentation.

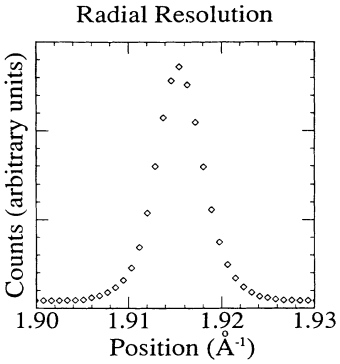

FIG. 10. Scan of Ge (111) used to measure instrumental resolution in the radial direction. The graph shows only the central portion of the scan; many more points were taken in the tails.

come narrower. In order to extract physically relevant information from the data, it is necessary to deconvolve instrumental and other system effects as discussed in detail below.

III. ANALYSIS

One of the purposes of this work was to consider the growth kinetics in an anisotropic system. Noda, Nishihara, and Yamada[27] measured the (110) superlattice peak in Cu_3Au by time-resolved x-ray-scattering techniques. They found evidence for scaling of $S(\mathbf{Q},t)$, a Lorentzian-squared line shape, and curvature-driven growth.

One is interested in the intrinsic line shape as well as the peak height and width. The instrumental resolution and mosaic were independently determined as discussed above. Measuring the intrinsic line shape of $S(\mathbf{Q},t)$ is also complicated by contributions to the linewidth, arising from the effects of finite grain size and strain. Estimates of broadening from these effects were made using measurements of the fundamental Cu_3Au Bragg peaks,[83] in particular, when the contribution to the width of the (010) arising from finite size and strain was estimated from radial scans of the (020) and (040). These scans were fitted with Gaussian profiles, and the resulting widths were corrected for instrumental resolution, assuming the widths add in quadrature ($\sigma_{\rm cor}=\sqrt{\sigma^2_{\rm measured}-\sigma^2_{\rm res}}$).

Ultimately the effects of finite grain size and strain can be included in an effective resolution function. Finite grain size leads to an identical contribution to the reciprocal space linewidth of each Bragg peak scattered from the sample. Strain can be viewed as providing a distribution of lattice constants, leading to an additional width at each peak that is linearly proportional to Q. To obtain the contribution to the width at the (010) arising from finite size and strain the (020) and (040) corrected widths were converted into units of inverse angstroms and fit to $a+bQ$, where a and b are fit parameters and Q is the magnitude of the corresponding scattering vector. The widths due to finite size and strain correspond to a and bq, respectively. The result of this fit suggested that the correction at the (010) was 0.002 $Å^{-1}$ (FWHM), one-third that of the instrumental resolution. One could argue that the widths should be added as $a+bQ^2$, not linearly as was done. If the fits are done this way the correction for finite size and strain becomes 10% larger and the overall correction 1.4% larger. The simplest correction is what was done, this method is equivalent to assuming the widths add like Lorentzian widths. The case for using $a+bQ^2$ assumes the widths add like Gaussian widths and that the width from strain is small compared to that for finite size, both of which are poor assumptions. In any case the final result was shown to be insensitive to the choice.

Mosaic spread is a measure of the distribution of orientations of the grains in the sample. Although both radial and transverse scans are affected by finite size and strain, only the transverse scans are strongly affected by mosaic spread. The mosaic spread contributes a constant angular width in real space to each peak. In reciprocal space the added width is proportional to Q.

The instrumental resolution (Fig. 10), finite size, and

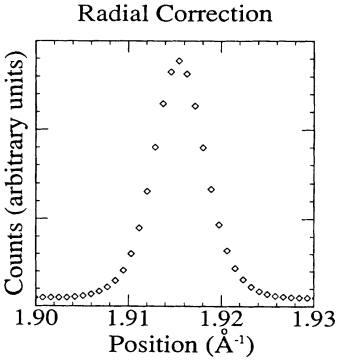

FIG. 11. Convolution of the instrumental resolution (Fig. 10) with a Gaussian of width 0.001 $Å^{-1}$ (0.002 $Å^{-1}$ FWHM) representing finite size and strain. The convolution represents the correction in the radial data.

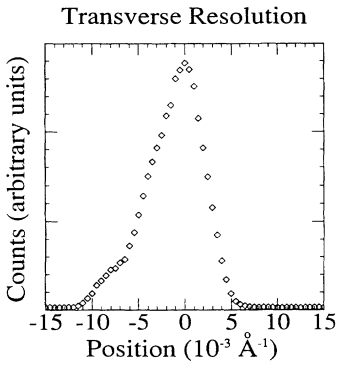

FIG. 12. Scan of Ge (111) used to measure instrumental resolution in the transverse direction.

strain were combined to yield an effective resolution function for the radial direction. This was done by numerically convolving the measured Ge (111) profile with a Gaussian line shape representing the sample effects. The resulting function is shown in Fig. 11. The scan of the Ge (111) used to measure the instrumental resolution in the transverse direction is shown in Fig. 12. The same procedure was used to give an effective resolution function for the transverse scans (Fig. 13), except that the mosaic effect was also incorporated.

Given the resolution function $R(\mathbf{Q},\mathbf{Q}')$, the measured scattering at momentum transfer $\mathbf{Q}$ is proportional (apart from trivial factors) to the convolution of the resolution function with the intrinsic $S(\mathbf{Q},t)$:

$$I(\mathbf{Q},t) \propto \int R(\mathbf{Q},\mathbf{Q}')S(\mathbf{Q}',t)d^3Q' \ . \tag{4}$$

Nucleation is associated with very early times and the equilibration of short-range order. The short-range-order peak intensity is very low, consequently only its existence could be seen. However, changes during the growth stage that are revealed through changes in the shape of the scattered intensity are seen. This change is analyzed by fitting the data to both theoretical and fundamental functions. Another method for seeing changes in line shape is to scale peaks from different times by their amplitude and width. In such scaling plots, differences in shape are apparent. However, they do not define or systematize the change as do the fits.

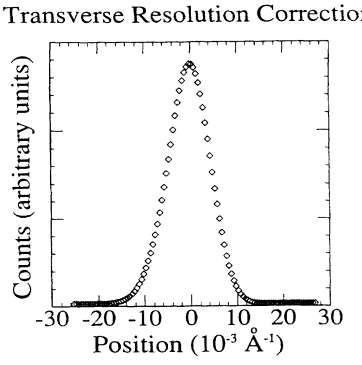

FIG. 13. Convolution of the instrumental resolution (Fig. 12), mosaic spread [Fig. 7 corrected to correspond to the (010)], and a Gaussian of width 0.001 Å^{-1} (0.002 Å^{-1} FWHM) representing finite size and strain. The convolution represents the correction in the transverse direction.

The fits to the data are used to extract a reciprocal space linewidth which is inversely proportional to an ordered domain size $L(t)$. $L(t)$ is then fitted to a power law in order to determine the time dependence. The fits also provide an amplitude and integrated intensity (width multiplied by the amplitude) as functions of time and temperature. Scaling the intensity and time gives information relating to changes, or lack thereof, in the mechanisms for growth.

Using least-squares fitting, the measured profiles were compared to the numerical convolution of the known resolution function with several model line shapes, including Gaussian, Lorentzian, Lorentzian squared, Lorentzian to a variable power, Hendricks-Teller model[66] (HT), and the theory of Ohta, Jasnow, and Kawasaki (OJK).[19] The definitions of the fitting functions are listed in the Appendix. We note that as a preliminary step,[91] the linewidths were extracted by fitting with the unconvolved model functions and corrected for the effective resolution by straightforward subtraction. Although in practice this method is accurate at early times when the profiles are broad, it leads to a systematic error as the profile widths become compatible to that of the effective resolution.

IV. DISCUSSION

Immediately after a high-temperature (700 °C) anneal a quench to T_f close to T_c is followed by a noticeable delay before any increase in scattering is observed. It is natural to associate this delay time with an incubation period for nucleation. However, after several quenches with short anneals at 20–40 °C above T_c the apparent delay time becomes shorter. In general the delay is longer for shallower quenches. The apparent delay can be quite striking. For quenches soon after a high-temperature anneal to $\sim$5 °C below T_c delays of up to half an hour are seen. One postulated origin for lengthy incubation times is the effect of elastic energies.[97] If this is indeed true, the history dependence observed here suggests that the delay time may be shortened by the introduction of preferred sites for inhomogeneous nucleation, possibly by the formation of defects upon repeated cycling of the sample between the ordered and disordered states. The behavior at very early time was the subject of a subsequent study reported elsewhere.[98] Such delays have been clearly observed in single grains of Mg_3In by Konishi and Noda.[99] In light of the history dependence discussed above, it is not too surprising that the deepest quench in which a delay is seen ($T_c - T \sim 5$ °C) is the first one after etching and annealing at 700 °C. After the delay the intensity is observed to rise linearly with time, corresponding to a period of rapid domain growth. At late times the intensity starts to saturate, asymptotically approaching some maximum $[I_\infty(T)]$ that increases with decreasing temperature.

TABLE I. Illustrative values of a χ^2 fit to functional form plus second-order polynomial background.

Line-shape function \ Transverse	$T=370.8\,^{\circ}C$ [$\chi^2=\sum (I_{fit}-I_{meas})^2/(n_{pnt}-n_{par})$] 8 min	23 min	48 min	123 min
Gaussian	2.1	22.2	31.6	22.1
Lorentzian	111.1	189.2	136.0	48.4
(Lorentzian)^2	25.8	8.3	3.4	2.7
(Lorentzian)^m [a]	(209.4) 2.1	(3.0) 2.0	(2.3) 2.6	(1.7) 2.1
HT	125.5	196.2	127.5	51.8
OJK[b]	126.6	213.2	169.4	81.6

[a]Values in parentheses represent the power m.
[b]Not convolved with the resolution function.

At very early times the line shape is similarly found to depend somewhat on the sample history. This was discovered after repeatedly cycling the sample through various quenches from starting points just above T_c to $T_f < T_c$. Before each cycle the sample was given a long anneal at a high temperature. The late-time behavior is much less dependent on the sample history. After the passage of any delay, and almost immediately after a deep quench ($\Delta T > 10\,^{\circ}C$), a broad Gaussian peak is seen. Initially the peak height grows relatively rapidly with time. As the height grows, the line shape crosses over to approximately a Lorentzian-squared shape.

Table I lists representative goodness of fit parameters (χ^2) for fits to various model line shapes (defined in the Appendix) for different times after a quench. The quoted χ^2 is the sum of the squares of the deviation divided by the degrees of freedom in the fit. A much more extensive table is published elsewhere.[92]

The crossover from a Gaussian to a Lorentzian-squared shape is depicted in Fig. 14. This seems to be a general feature of the ordering process, and has also been observed in kinetics of the ordering transition in

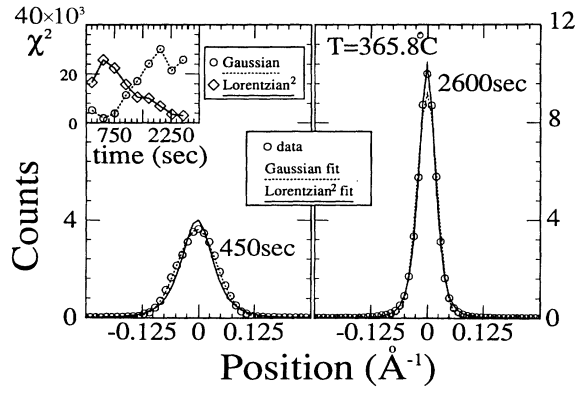

FIG. 14. Change in the line shape after a quench. Transverse scans of the (010) with $a^*=1.666$ Å^{-1}. Solid (dotted) line is a Lorentzian-squared (Gaussian) convolution least-squares fit. The FWHM of the instrumental resolution is equal to the width of the tick marks on the position axis. A similar figure using nonconvolution fits was published in Ref. 91. Inset: χ^2 (as defined in text) of the fit vs time for the Gaussian (circles) and Lorentzian-squared (diamonds) fits.

$(TMTSF_2)ClO_4$.[100] A kinetic line shape crossover has also been observed in a random antiferromagnetic system,[101] but the details differ. In fact, the details of the crossover also depend on sample history. A quench from $T_i=420\,^{\circ}C$ to $T_f=375\,^{\circ}C$ immediately after a high-temperature anneal showed the persistence of the Gaussian shape for up to 17 min. An identical quench to $375\,^{\circ}C$ was repeated ten times in a row without an intermediate high-temperature anneal. The duration of the Gaussian regime was shorter with each subsequent quench, and eventually was less than 5 min. Unfortunately, it was not possible to follow the evolution of the line shape on time scales less than 5 min because the uncertainty arising from counting statistics became too large to allow the shape to be accurately determined. Following an anneal at $700\,^{\circ}C$ for 8 h, the line shape crossover was repeatable. In general, immediately after a high-temperature anneal, the crossover is more apparent for deeper quenches, but this has not been tested for quenches to temperatures less than $350\,^{\circ}C$.

At late times, the line shape is essentially a Lorentzian squared. Several theoretical predictions on coarsening suggest[19,23] that the tails of $S(q,t)$ should decay as q^{-4}, consistent with a Lorentzian-squared peak. The theory of Ohta, Jasnow, and Kawasaki[19] (OJK) derives an equation for the line shape that involves an integration for each q. Using numerical integration, nonconvolution fits to this line shape have been done on selected peaks from quenches to various temperatures and times such that the resolution is small compared to the overall width. However, the resulting fits during coarsening were significantly worse than the Lorentzian-squared fits for the transverse scans but only slightly worse for the radial scans. Definitions for this theory and all line shapes discussed are summarized in the Appendix. Keeping in mind that the justification for assuming a Lorentzian-squared peak has always been that the tails decay as q^{-4} as OJK theory predicts, it is somewhat surprising that a Lorentzian-squared shape actually fits better than the full theory. However, several approximations were made in the theory that may explain this. The theory assumes an isotropic system, and a Gaussian distribution of fluctuations of the domain-wall positions. The authors point out the dependence of their results on the choice of this distribution.[19]

The Lorentzian-squared line shape can be caused by

ordered domains separated by sharp walls.[102] The falling off as q^{-4} (Prod's law) arises naturally in most theories of coarsening in a system with a nonconserved order parameter. The Lorentzian-squared line shape is a clear signature of the late-stage coarsening (and, in this case, nonequilibrium scaling) regime. The late-time scaling as well as the change in the line shape of $S(\mathbf{q},t)$ is easily seen. If the peaks were the same shape, plots of counts divided by the fitted amplitude vs position divided by the width, would lie on the same curve. Figure 15 shows some of the raw data for the transverse 375.6 °C quench with Lorentzian-squared fits to all but the earliest one, which is fit to a Gaussian. Figure 16 shows the data after being scaled, the two lines are a scaled Lorentzian-square fit and a scaled Gaussian fit. The scaled data demonstrates two things; first, the earliest peak has a different shape (Gaussian) than all the rest, and second, the late-time scaling regime of $S(\mathbf{q},t)$.

The simplest model for superlattice peak line shapes in Cu_3Au is a Hendrichs-Teller[103] (HT) approach, which assumes independent domain walls. The predicted scattering function[66] in this approximation is an anisotropic Lorentzian in the small-$|\mathbf{q}|$ limit. The function definition is presented in the Appendix. This HT approach was used by Ludwig *et al.*[66] to parametrize early-time kinetic experiments on Cu_3Au. The small-$|\mathbf{q}|$ limit is a modified Lorentzian where the linewidth depends on the direction in $\mathbf{k}$ space. Although this approach effectively parametrized their data it would not do so here. However, this is not a contradiction because all of their scans were taken in the time it took to take our first scan, the resolution they used was very broad compared to the present work, and their sample was a polycrystalline wire. The modified Lorentzian produced poorer fits to our data than a straight Lorentzian, which did not fit well at any time. However, if the shape was convolved with the resolution function the fits were poor but acceptable. It is worth noting that the background for these fits was constrained to be positive; if negative backgrounds were permitted considerably better fits were found in the transverse scans, which contained considerably few points in the tails compared to radial scans.

In addition to the above-mentioned fitted line shapes, the scans were also fitted to a pure Lorentzian and a Lorentzian to a variable power. The difference in the χ^2 values between the Lorentzian squared and Lorentzian to the mth power during coarsening is never so great as to make one believe that the peak is not a Lorentzian-squared shape. In fact, the dependence of the χ^2 on m is relatively flat between about 1.3 to over 3 but rises quickly near 1.0.

The Gaussian line shape seen at early times can be understood if small ordered domains within a disordered matrix scatter incoherently. The history dependence might be explained, if after cycling, the system rapidly nucleates many smaller domains which meet at an earlier time resulting in the Lorentzian-squared line shape. While there is no direct evidence for this picture, it is consistent with the disappearance of the shallow quench incubation time upon cycling.

A recent study by Torii, Tamaki, and Wakabayashi[104] showed that for very shallow quenches (extending to roughly 4.5 °C below T_c) the superlattice peak at late times consists of a sharp Bragg-like component superimposed on a very broad Lorentzian peak. Since this exists at temperatures where a significant portion of the sample is always disordered, it is natural to interpret the broad component as arising from short-range-order fluctuations. We have also observed a two-component line shape in studies of sputtered films[105] and a subsequent study of shallow quenches.[98] There is evidence that the disordered volume of the sample will be primarily at the surface.[106–108] It is not clear whether the two com-

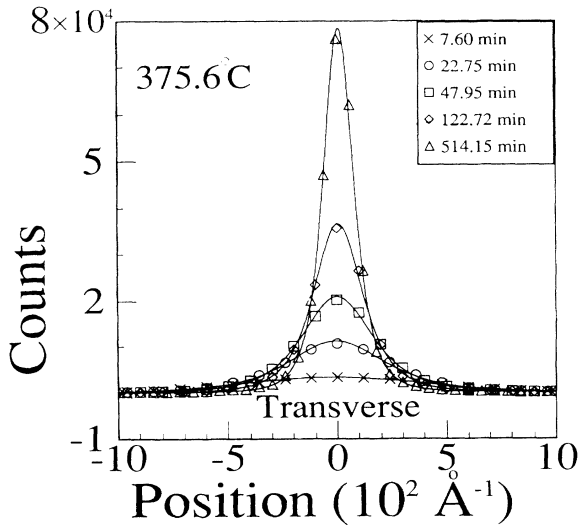

FIG. 15. Raw data on the (010) bulk superlattice diffraction peak. Solid lines are fits to the data. For the 7.60-min scan a Gaussian fit is shown, the rest are Lorentzian-squared fits.

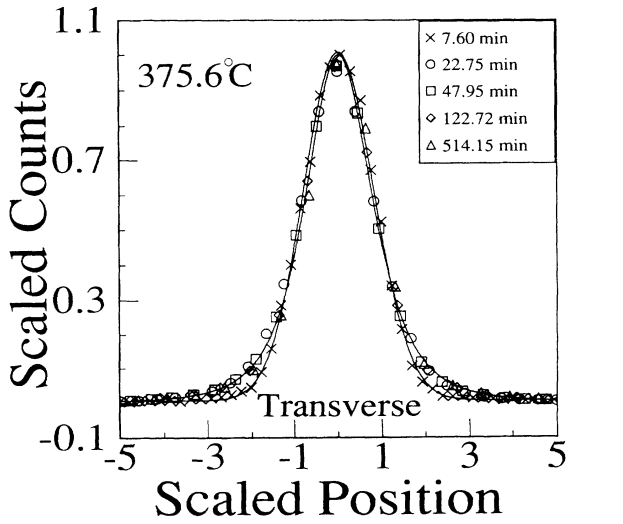

FIG. 16. Data shown in Fig. 15 scaled by amplitude and width. The solid lines describe a Gaussian and a Lorentzian-squared shape. The 7.60-min peak is Gaussian, the rest are Lorentzian squared.

ponents are coming from two different volumes or not. The observed crossover in line shape from Gaussian to Lorentzian squared is not connected with this two-component line shape. The crossover in line shape is seen for deeper quenches, and is less apparent at temperatures closer to T_c where the effects from a short-range-order peak were seen to be more pronounced. Moreover, a study of the evolution of the short-range-order[66] component shows that, in the temperature range we discuss here, the short-range-order component equilibrates much faster than the line shape evolution occurs.

The line shapes observed here are roughly consistent with Lai's[88] theory for kinetics in the Cu_3Au system. The early-time linear regime in this theory predicts a Gaussian line shape in a way similar to the linear theory of spinodal decomposition. Recently Lai has developed a coarse-grained model of the phase transition. At late times this model predicts a modified Lorentzian squared of the form,

$$F_1(k)=\frac{1}{(1+b_1k^2)^2+2b_2k^2} . \quad (5)$$

Fits of this form to our data do not favor this form over that of a pure Lorentzian squared ($b_2=0$). However, Lai points out that this variance could be due to finite-size effects in the numerical computations for this model. Lai also suggested that the model may not be "completely settled into the longest time asymptotic regime." Recalling that during the crossover there is a period where the peak is neither Gaussian or Lorentzian squared, our fits were checked to see if b_2 could be related to the crossover. However, there was no evidence of b_2 contributing in any systematic way. In fact, even at the crossover this modification has very little effect on the shape of the fit. Nevertheless this model exhibits the qualitative behavior that we have observed.

A plot of amplitude vs time is shown in Fig. 17. The amplitude used in the plot is the convolution-fitted amplitude and as such is corrected for resolution effects in the direction of the scan. The amplitude should be proportional to the square of the order parameter and here should scale as $[L(t)]^d$. Assuming curvature-driven growth, the amplitude should have a time dependence $t^{d/2}$. However, the data has only been corrected for resolution effects in one direction and the effective measurement approximately integrates over the other two dimensions, therefore, the measured amplitude should roughly scale as $[L(t)]^{d-2}$ and have a time dependence of $t^{1/2}$. A plot of $\log_{10}$ (amplitude) vs $\log_{10}$ (time) is shown in Fig. 18. The late-time slope for the deeper quenches is 0.46, a value close to the value found for the time dependence of L as discussed below. Trying to extract the time dependence of L from the amplitude is not a good method due to the uncertainty of the resolution effect. However, it is interesting that a value close to the expected value of $\frac{1}{2}$ is found, indicating that the scaling involved is as expected from theory. The curvature in the log-log plot is at least in part due to the resolution function.

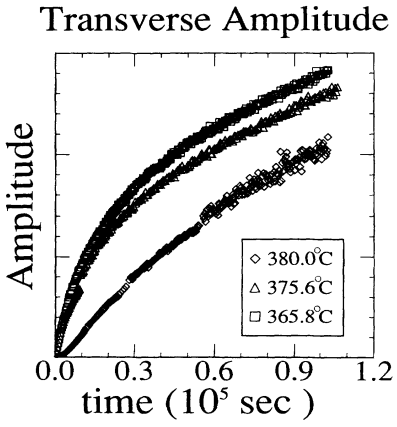

FIG. 17. Convolution fitted amplitude vs time for the temperatures shown. The delay seen in the plot of the integrated intensity is also seen here.

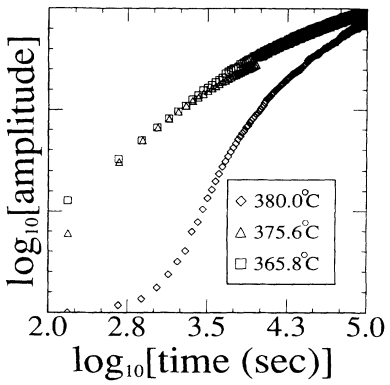

FIG. 18. $\log_{10}$ (amplitude) vs $\log_{10}$ (time) for the same data shown in Fig. 17.

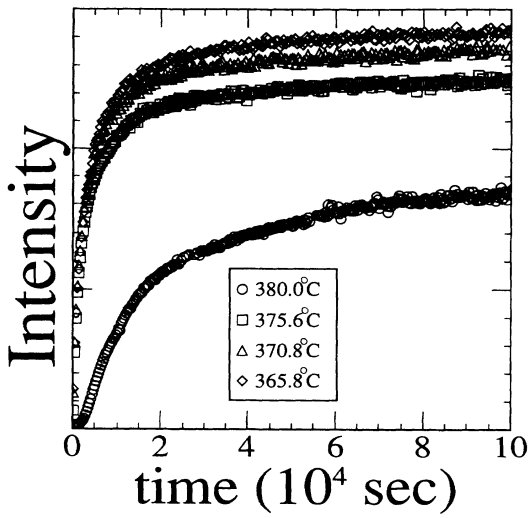

FIG. 19. Intensity (width of convolution fits multiplied by the amplitude of the fit) vs time. The 380.0 °C data shows a delay of approximately 1900 sec that corresponds to a period of nucleation. The data shown was taken in the transverse direction at the (010).

Figure 19 displays the integrated intensities (fitted amplitude multiplied by fitted width) vs time after a thermal quench for the transverse directions at several temperatures. The 380.0 °C transverse data shows a delay immediately after the quench, as observed in many other quenches to temperatures closer to T_c. Figure 20 shows the data from Fig. 19 scaled by plotting I/I_∞ vs t/b where b is the time for the intensity to reach $I_\infty/2$. As expected,[27] the data falls on a universal curve.

From a simplistic Ising-model calculation it might be argued that the integrated intensity should be constant and that in Figs. 8, 9, and 19 the rise in integrated intensity is due to the resolution function integrating over more of the peak as the peak becomes narrower. This is not the case. First of all, the integrated intensity is calculated from the product of the fitted width and the fitted amplitude, not from the sum of all the counts. Hence, the intensity in the tails is accounted for (at least in the direction scanned). Figure 21 shows the integrated intensity, amplitude, and constant background as a function of time. In this multiple plot the background has been multiplied by 1000 to plot it on the same scale as the amplitude. The fact that the fitted background is 1000 times or more smaller than the fitted amplitude implies that the missing intensity would have to be spread out in a volume 10^3 times larger than what was effectively covered. It is obvious that some of the intensity is being falsely counted as the background due to the rise in the background with time. However, this change in fitted background is in the wrong direction because the argument says intensity is missing at early times, not late. This is a different problem that is discussed in connection with power-law growth. The background should probably be quadratic due to a diffuse peak arising from thermal fluctuations. Moreover, the fitted background for the second and third

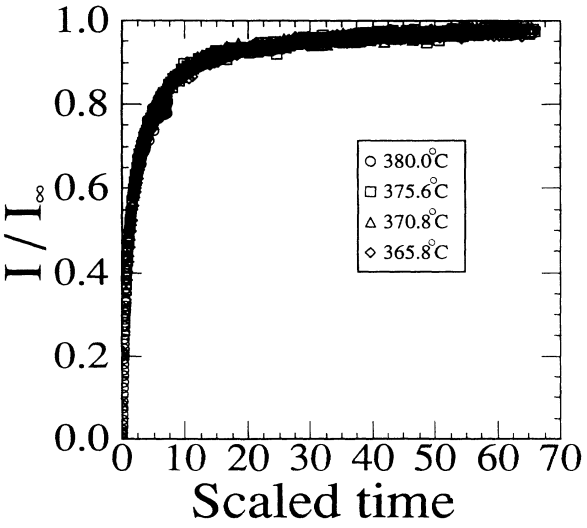

FIG. 20. Scaled intensity (I/I_∞) vs scaled time ($t/t_{\infty/2}$ where $t_{\infty/2}$ is the time the intensity reached one-half its late-time asymptotic value of I_∞). The nucleation period for the 380.0 °C data was subtracted from the time before scaling. The unscaled data are in Fig. 19.

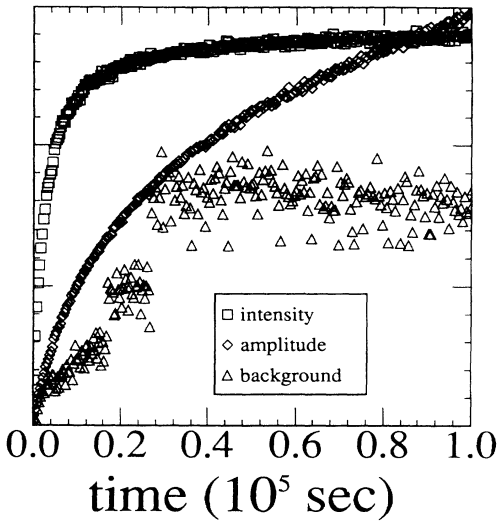

FIG. 21. Plots of integrated intensity, amplitude, and fitted constant background. The background has been multiplied by 10^3 in order to plot it on the same scale as the amplitude. The integrated intensity has also been scaled to fit on the graph.

points is slightly negative, once again indicating that the change in intensity is greater than suggested by the plots.

The above argument shows that any missing intensity cannot be coming from the direction that was scanned. The resolution function in the vertical direction is large, which strongly implies that any missing intensity is lost in the radial direction. As it happens, several quenches with radial scans using the graphite monochromator and analyzer (what has been called the transverse setup) were tried. The resolution in that direction turned out to be too large; within an hour after a quench the instrument was resolution limited. The width after 6 h suggests that the resolution was close to 0.02 Å^{-1} (FWHM). Remember that at the (010) the radial direction probes the thin part of the scattering disk. Based on this value for the radial resolution, the intrinsic peak width is equal to the instrumental resolution width 16 min after the quench. At this point the peak should be almost completely integrated over (for the deeper quenches). Some of the intensity could still be lost in the tails due to differences in line shapes. The intrinsic line shape at this time is approaching that of a Lorentzian squared and the instrumental resolution (Fig. 12) is something between a Gaussian and a Lorentzian squared. A time of 16 min corresponds to the fourth point in Fig. 21, which has an intensity of 35% of the final intensity. Hence, about 65% of the change in intensity is real. An even stronger argument can be made for the radial data. A change in integrated intensity has also been seen in other systems by Wakabayashi.[109,110]

Figure 22 shows a plot of $\log_{10}(L)$ vs $\log_{10}(t)$ whose slope is the power for the time dependence of the domain size [a in Eq. (3)]. In Table II are listed the exponents a for curvature-driven growth, as a function of temperature and the order of the polynomial background used in the

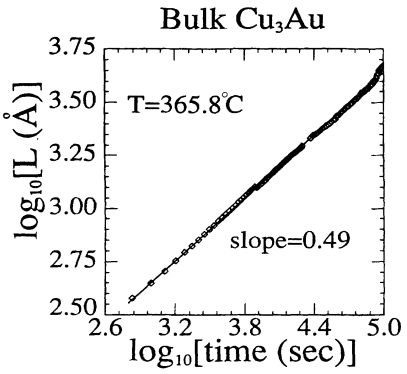

FIG. 22. Log_{10} (length) vs $\log_{10}$ (time after the quench). $L \propto 2\pi/\Gamma$, where Γ is the Lorentzian-squared-fitted width. The solid line is a linear fit whose slope corresponds to the exponent a for power-law growth.

fitting. For the radial data the order of the polynomial background was not important because only the constant term gave any sizable contribution. The exponent for the radial data was found to be 0.50 ± 0.03 and temperature independent. Here, the error in a was estimated from the effect of changing the resolution correction, as well as the standard deviation as calculated from values at different temperatures, which was 0.014. An error in the resolution correction would contribute a systematic error; however, this correction as discussed earlier is dominated by the instrumental resolution, which is well known. This is not the case in the transverse direction, where the resolution correction is less well defined due to the addition of the mosaic spread, and the order of the polynomial background seems to affect the result.

It should be noted that the 380 °C transverse data is inconsistent with all the other data, yielding a significantly larger exponent than the others. We believe it is possible that there is a small systematic underestimate of the transverse exponent in the other quenches arising from a change in the instrumental resolution. The 380 °C data was from the first quench after etching and annealing of the sample, and hence can be separated temporally from the rest of the data. Late in the series of quenches the filament in the x-ray source burned out and was replaced. Changes in the filament before failing may be important, in fact the exponents a can be correlated to the order in which the data was collected. The value obtained for a in the transverse direction decreases with time until the filament was replaced then goes up. This could be a result of the filament sagging with time (a common occurrence immediately before failure), and hence changing the effective resolution. The filament was replaced before the 382 °C quench and after all the others listed in Table II. Consequently, the instrumental resolution, which was measured after the series is better known for the 382 °C data. Movement of the x-ray beam due to filament sagging would have at least two effects: it would very slightly change the area of the sample considered, perhaps altering the mosaic, and it would misalign the sample. However, the most likely way that the resolution would be changed is simply by increasing the spot size on the anode that the x rays are emitted from. A lower value for a would be consistent with an under correction for the true instrumental resolution. Furthermore, the change in a cannot be correlated with temperature. The systematic errors arising from uncertainties in the resolution correction probably outweigh the statistical errors. We would guess the uncertainty to be around 10% based on differences obtained by changing the modeling of the background.

The possibility of a lower exponent for the transverse data is suggestive of problems with impurities or incorrect stoichiometry. Random imperfections lead to slower growth, possibly a $\log(t)$ growth law.[77,79,80,105] This is very unlikely due to the limits placed on the stoichiometry that were discussed earlier. In addition, the radial data does not show these minor inconsistencies. We believe that all of the data is consistent, within experimental error, with $a=\frac{1}{2}$, the canonical value for curvature-driven growth.

V. CONCLUSIONS

The development of order in the bulk single-crystal Cu_3Au sample after a thermal quench from the disordered state exhibits three distinct regimes: nucleation,

TABLE II. Exponents a for power-law growth [Eq. (3)].

Direction background	Constant	Transverse Linear	Quadratic	Radial Constant
Temperature (°C)		a		
382.0	0.45	0.47	0.49	0.49
380.0	0.54	0.56	0.58	
375.6	0.40	0.40	0.45	0.51
370.8	0.42	0.43	0.46	0.51
365.8	0.40	0.43	0.46	0.49
Average	0.44	0.46	0.49	0.50
std. dev.	0.06	0.06	0.05	0.01

ordering, and coarsening. The first is characterized by a Gaussian structure factor associated with small ordered domains embedded in a disordered matrix. At the beginning of the ordering regime, the shape is Gaussian but quickly crosses over, becoming rapidly more Lorentzian squared with time. At the onset of coarsening the structure factor is very well described by a Lorentzian-squared function. During coarsening, domain growth is consistent with a curvature-driven growth law for both type-1 and type-2 walls. Moreover, the power a associated with this growth has been found to be 0.5 to a high degree of accuracy in the radial direction (type-2 walls) and to a lesser degree in the transverse direction, implying that scaling during coarsening is valid in an anisotropic system. However, the change in line shape clearly shows that $\mathbf{S}(\mathbf{Q},t)$ can only be scaled during coarsening and not during ordering. This fact is easily seen by viewing the disordered phase as a thick domain wall, in which case the size of the wall relative to the ordered domain size would be different for different times so that scaling would not exactly recreate the state of the system. Our data is qualitatively described by the theory recently put forth by Lai based on a three-component order parameter. This theory produces a slightly modified Lorentzian-squared structure factor at late times and a Gaussian shape at early times. Although a change in the line shape exists in Lai's theory the history dependence of this change is not explained. However, the level of short-range order and its effect on nucleation is likely to play an essential role in explaining the history dependence. It is possible that a previously well ordered sample which has been disordered close to the transition temperature (within $\approx 40\,^{\circ}\mathrm{C}$) has a more homogeneous nucleation. If nucleation takes place throughout the sample with a high density of nucleation sites, then the system would reach coarsening very rapidly and have a short ordering regime.

As discussed earlier, the history dependence of the line-shape crossover is not understood. Its likely connection with the nucleation process is an interesting problem that may broaden our understanding of how short-range order affects the transition. In addition, there seems to be little information regarding the ordering stage. Further investigations on this intermediate stage would be informative.

ACKNOWLEDGMENTS

This work has been supported by U.S. DOE under Grant No. DE-FG05-91ER45280. We thank M. Singh, P. Kumar, M. Sutton, M. Grant, G. Mazenko, Z. Lai, J. Gunton, and N. Wakabayashi for useful discussions. We also thank W. Ruby for expert technical assistance.

APPENDIX: FUNCTIONAL DEFINITIONS USED IN FITTING

In the following, x is the position coordinate, and x_0 is the position of the peak. Here and throughout the text σ is used to represent a Gaussian width and Γ a width for a Lorentzian to any power. The following definitions are such that the widths will approximately equal a HWHM. The amplitude is A.

Gaussian,

$$F(x)=A\exp\{[(x-x_0)/2\sigma]^2\}\ ; \tag{A1}$$

Lorentzian,

$$F(x)=\frac{1}{1+[(x-x_0)/\Gamma]^2}\ ; \tag{A2}$$

Lorentzian squared,

$$F(x)=\{1+\tfrac{1}{2}[(x-x_0)/\Gamma]^2\}^{-2}\ ; \tag{A3}$$

Lorentzian to the mth power,

$$F(x)=\{1+\tfrac{1}{2}[(x-x_0)/\Gamma]^2\}^{-m}\ ; \tag{A4}$$

HT Theory,[66]

$$I(\mathbf{k})=\frac{2}{3}(f_{\mathrm{Au}}-f_{\mathrm{Cu}})\sum_{i\neq j\neq l=1}^{3}\Gamma_{i2}\Gamma_{j2}\Gamma_{l3}[1+\cos(\pi k_j)-2\cos(\pi k_l)]\ , \tag{A5}$$

where

$$\Gamma_{im}=(1-x_m^2)/[1+x_m^2-2x_m\cos(2\pi k_i)]\ ,$$

$$x_2=(1-2\eta-2\gamma),\quad x_3=(1-4\eta)\ .$$

γ is the probability of finding a type-1 wall between two unit cells. 2η is the probability of finding a type-2 wall between two unit cells.

At the (010), a transverse direction is (x00) and $k_1=ax/2\pi$, $k_2=1$, and $k_3=0$. Equation (A5) then reduces to

$$A(1+C\{1-\cos[a(x-x_0)]\})^{-1}\ , \tag{A6}$$

where

$$C=[0.5-(\eta+\gamma)^2]/(\eta+\gamma)\ ,$$

$$A=\mathrm{Am}(\eta,\gamma,f_{\mathrm{Au}}-f_{\mathrm{Cu}})$$

are fit parameters.

In the radial direction $k_1=0$, $k_2=a(1+x)/2\pi$, and $k_3=0$. This leads to

$$I(k_2)=A\frac{\cos(\pi k_2)-1}{1+D[1-\cos(2\pi k_2)]}\ , \tag{A7}$$

where

$$k_2=2.487\,885\,6\sin[0.413\,643\ \mathrm{rad}+(x-x_0)\times 2.181\,661\,6\times 10^{-4}\ \mathrm{rad/PSD\ channel}]\ ,$$

x is in PSD channels, 0.4136 is the position of the (010) in radians, and 2.48 . . . is a/λ.

OJK theory,[19]

$$I(x)=\frac{2}{\pi}\frac{(2\pi)^{1.5}}{x}\int_0^\infty dR\frac{R^3 J_{3/2}(xR)}{\{xR[\exp(R^2)-1]\}^{1/2}}\ , \tag{A8}$$

where $J_{2/3}$ is a Bessel function. In the fitting routine $x=(x-x_0)/\Gamma$ is approximated as $10.47(1-x^2)$ if the absolute value of $x<10^{-4}$. Copies of the fitting and numerical integration routines used can be found in Ref. 111.

[1]J. D. Gunton, M. San Miguel, and P. S. Sahni, in *Phase Transitions and Critica Phenomena,* edited by C. Domb and J. L. Lebowitz (Academic, London, 1983), Vol. 8.

[2]J. D. Guton, in *Magnetic Phase Transitions,* edited by M. Ausloos and R. J. Elliott (Springer, Berlin, 1983).

[3]K. Kawasaki, in *Phase Transitions and Critical Phenomena,* edited by C. Domb and M. S. Green (Academic, New York, 1972), Vol. 2.

[4]J. W. Christian, in *The Theory of Transformations in Metals and Alloys, Part 1,* edited by D. W. Hopkins (Pergamon, New York, 1975).

[5]M. F. Collius, in *Magnetic Critical Scattering,* edited by S. W. Lovesey and E. W. J. Mitchell (Oxford University Press, New York, 1989).

[6]H. E. Stanley, in *Introduction to Phase Transitions and Critical Phenomena,* edited by W. Marshall and D. H. Wilkinson (Oxford University Press, New York, 1971).

[7]J. D. Guton, J. Stat. Phys. **34**, 1019 (1984).

[8]G. F. Mazenko, Phys. Rev. B **26**, 5103 (1983).

[9]G. F. Mazenko and O. T. Valls, Phys. Rev. B **27**, 6811 (1983).

[10]G. F. Mazenko and O. T. Valls, Phys. Rev. Lett. **51**, 2044 (1983).

[11]G. F. Mazenko and O. T. Valls, Phys. Rev. B **30**, 6732 (1984).

[12]F. C. Zhang, O. T. Valls, and G. F. Mazenko, Phys. Rev. B **31**, 1579 (1985).

[13]G. F. Mazenko, O. T. Valls, and F. C. Zhang, Phys. Rev. B **31**, 4453 (1985).

[14]Z. W. Zai, O. T. Valls, and G. F. Mazenko, Phys. Rev. B **37**, 9481 (1988).

[15]I. M. Lifshitz and V. V. Slyozov, J. Phys. Chem. Solids **19**, 35 (1961).

[16]J. W. Cahn and J. E. Hilliard, J. Chem. Phys. **28**, 258 (1958).

[17]J. S. Langer, M. Bar-On, and H. D. Miller, Phys. Rev. A **11**, 1417 (1975).

[18]K. Kawasaki, M. Yalabik, and J. D. Gunton, Phys. Rev. A **17**, 445 (1978).

[19]T. Ohta, D. Jasnow, and K. Kawasaki, Phys. Rev. Lett. **49**, 1223 (1982).

[20]M. Grant and J. D. Gunton, Phys. Rev. B **29**, 1521 (1984).

[21]G. T. Gawlinski, M. Grant, J. D. Gunton, and K. Kaski, Phys. Rev. B **31**, 281 (1985).

[22]A. Milchev, K. Binder, and D. W. Heerman, Z. Phys. B **63**, 521 (1986).

[23]G. Mazenko, O. T. Valls, and M. Zannetti, Phys. Rev. B **40**, 379 (1989).

[24]H. L. Snyder and P. Meakin, J. Chem. Phys. **79**, 5588 (1983).

[25]T. Hashimoto, K. Nishimura, and Y. Takeuchi, Phys. Lett. **65A**, 250 (1978).

[26]S. Nishihara, Y. Noda, and Y. Yamada, Solid State Commun. **44**, 1487 (1982).

[27]Y. Noda, S. Nishihara, and Y. Yamada, J. Phys. Soc. Jpn. **53**, 4241 (1983).

[28]Y. Yamada, N. Hayama, J. D. Axe, and S. M. Shapiro, Phys. Rev. Lett. **27**, 1655 (1984).

[29]O. Blaschko, P. Fratzl, G. Grest, M. Bernole, and G. Fuyara, Phys. Rev. B **30**, 6498 (1984).

[30]F. Furusaka, Y. Ishikawa, and M. Mera, Phys. Rev. Lett. **54**, 2611 (1985).

[31]M. Hennion, D. Ronzaud, and P. Guyot, Acta Metall. **30**, 599 (1982).

[32]P. K. Wu, J. H. Perepezko, J. T. McKinney, and M. G. Lagally, Phys. Rev. Lett. **51**, 1577 (1983).

[33]G. C. Wang and T. M. Lu, Phys. Rev. **50**, 2014 (1983).

[34]S. Katano and M. Iizumi, Phys. Rev. Lett. **52**, 835 (1984).

[35]H. Homma and R. Clarke, Phys. Rev. Lett. **52**, 629 (1984).

[36]M. Furusaka, Y. Ishikawa, S. Yamaguchi, and Y. Fusino, Physica B&C **120C**, 383 (1983).

[37]G. Kostnz, Physica B&C **120C**, 387 (1983).

[38]S. Katano and M. Iizumi, Physica B&C **120C**, 392 (1983).

[39]S. Komura, K. Osamura, H. Gujii, and T. Takeda, Physica B&C **120C**, 397 (1983).

[40]R. Clarke, Bull. Am. Phys. Soc. **30**, 346 (1985).

[41]D. B. McWhan, G. Aeppli, J. P. Remeika, and S. Nelson, J. Phys. C **18**, 2307 (1985).

[42]A. Bortz, M. H. Kalos, J. L. Lebowitz, and M. A. Zendegas, Phys. Rev. B **10**, 535 (1974).

[43]J. Marro, A. Bortz, M. H. Kalos, and J. L. Lebowitz, Phys. Rev. B **12**, 2000 (1975).

[44]A. Sur, J. L. Lebowitz, J. Marro, and M. H. Kalos, Phys. Rev. B **15**, 3014 (1977).

[45]J. Marro, J. L. Lebowitz, and M. H. Kalos, Phys. Rev. Lett. **43**, 282 (1979).

[46]M. K. Phani, J. L. Lebowitz, and M. H. Kalos, Phys. Rev. Lett. **43**, 368 (1980).

[47]P. S. Sahni and J. D. Gunton, Phys. Rev. Lett. **45**, 368 (1980).

[48]P. S. Sahni, G. Dee, J. D. Gunton, M. K. Phani, J. L. Lebowitz, and M. H. Kalos, Phys. Rev. B **24**, 410 (1981).

[49]J. L. Lebowitz, J. Marro, and M. H. Kalos, Acta Metall. **30**, 297 (1982).

[50]P. S. Sahni, G. S. Grest, and S. A. Safran, Phys. Rev. Lett. **50**, 60 (1983).

[51]A. Sadiq and K. Binder, Phys. Rev. Lett. **51**, 674 (1983).

[52]K. Kaski, M. C. Yalabik, D. J. Gunton, and P. S. Sahni, Phys. Rev. B **28**, 5263 (1983).

[53]G. S. Grest, D. S. Srolovitz, and M. P. Anderson, Phys. Rev. Lett. **51**, 634 (1983).

[54]A. Sadiq and K. Binder, J. Stat. Phys. **35**, 517 (1984).

[55]G. S. Great and P. S. Sahni, Phys. Rev. B **30**, 226 (1984).

[56]G. S. Grest and D. S. Srolovitz, Phys. Rev. B **30**, 5150 (1984).

[57]P. S. Sahni, G. S. Grest, M. P. Anderson, and D. S. Srolovitz, Phys. Rev. Lett. **50**, 263 (1983).

[58]S. A. Safran, P. S. Sahni, and G. S. Grest, Phys. Rev. B **26**, 466 (1982).

[59]G. S. Grest, S. A. Safran, and P. S. Sahni, J. Magn. Magn.

Mater. **31-34**, 1011 (1983).
[60]S. A. Safran, P. S. Sahni, and G. S. Grest, Phys. Rev. B **28**, 2693 (1983).
[61]P. S. Sahni, D. S. Srolovitz, G. S. Grest, M. P. Anderson, and S. A. Safran, Phys. Rev. B **28**, 2705 (1983).
[62]K. Huang, *Statistical Mechanics* (Wiley, New York, 1963).
[63]R. S. Glauber, J. Math. Phys. **4**, 294 (1963).
[64]K. Binder, Rep. Prog. Phys. **50**, 783 (1987).
[65]D. de Fontaine, in *Solid State Physics,* edited by H. Ehrenreich, F. Seitz, and D. Turnbull (Academic, New York, 1979), Vol. 34, pp. 210–216.
[66]K. F. Ludwig, Jr., G. B. Stephenson, J. L. Jordan-Sweet, J. Mainville, Y. S. Yang, and M. Sutton, Phys. Rev. Lett. **61**, 1859 (1988).
[67]B. D. Gaulin, E. D. Hallman, and E. C. Svensson, Phys. Rev. Lett. **64**, 289 (1990).
[68]H. Chen and J. B. Cohen, J. Phys. (Paris) Colloq. **38**, C7-314 (1977).
[69]L. Van Hove, Phys. Rev. **95**, 249 (1954).
[70]T. Hashimoto, K. Nishimura, and Y. Takeuchi, J. Phys. Soc. Jpn. **45**, 1127 (1978).
[71]T. Castan and P. A. Lindgard, Phys. Rev. B **41**, 2534 (1990).
[72]R. Peierls, Proc. R. Soc. London **154A**, 207 (1936).
[73]G. Vineyard, Phys. Rev. **102**, 981 (1956).
[74]S. M. Allen and J. W. Cahn, Acta Metall. **27**, 1085 (1979).
[75]I. M. Lifshitz, Zh. Eksp. Teor. Fiz. **42**, 1354 (1962) [Sov. Phys. JETP **15**, 939 (1962)].
[76]D. A. Huse and C. L. Henley, Phys. Rev. Lett. **54**, 2708 (1985).
[77]G. S. Grest and D. J. Srolovitz, Phys. Rev. B **32**, 3014 (1985).
[78]D. J. Srolovitz and G. S. Grest, Phys. Rev. B **32**, 3021 (1985).
[79]D. Chowdhury, M. Grant, and J. D. Gunton, Phys. Rev. B **35**, 6792 (1987).
[80]D. J. Srolovitz and G. N. Hassold, Phys. Rev. B **35**, 6902 (1987).
[81]D. G. Morris, Phys. Status Solidi A **82**, 145 (1975).
[82]P. J. Shah and O. G. Mouritsen, Phys. Rev. B **41**, 7003 (1990).
[83]B. Warren, *X-Ray Diffraction* (Addison-Wesley, Reading, MA, 1969), Chap. 12, pp. 206–250.
[84]R. Kikuchi and J. W. Cahn, Acta Metall. **27**, 1337 (1979).
[85]S. C. Moss, in *Local Atomic Arrangements Studied by X-Ray Diffraction,* edited by J. B. Cohen and S. E. Hilliard (Gordon and Breach, New York, 1966), p. 95.
[86]K. Binder, in *Statistical Physics,* edited by H. E. Stanley (North-Holland, New York, 1986).
[87]E. Domany, Y. Shnidman, and D. Mukamel, J. Phys. C **15**, L495 (1982).
[88]Z. W. Lai, Phys. Rev. B **13**, 9239 (1990).
[89]P. Kumar (private communication).
[90]F. P. Burns and S. L. Quimby, Phys. Rev. **97**, 1567 (1955).
[91]S. E. Nagler, R. F. Shannon, Jr., C. R. Harkless, M. A. Singh, and R. M. Nicklow, Phys. Rev. Lett. **61**, 718 (1988).
[92]R. F. Shannon, Jr., Ph.D. dissertation, University of Florida, 1990.
[93]R. A. Cowley, Acta Crystallogr. Sec. A **43**, 825 (1987).
[94]M. Hansen and K. Anderko, *Constitution of Binary Alloys* (reprinted by arrangement with McGraw-Hill by Genium, Schenectady, NY, 1985).
[95]W. Pearson, *A Handbook of Lattice Spacings and Structures of Metals and Alloys* (Pergamon, New York, 1958).
[96]C. A. Lucas, E. Gartstein, and R. A. Cowley, Acta Crystallogr. Sec. A **45**, 416 (1989).
[97]P. Chandra, Phys. Rev. A **39**, 3672 (1989).
[98]R. F. Shannon, Jr. (unpublished).
[99]H. Konishi and Y. Noda, in *Dynamics of Ordering Processes,* edited by S. Komura (Plenum, New York, 1988).
[100]J. P. Pouget, S. Kagoshima, T. Tamegai, Y. Nogami, K. Kubo, T. Nakajina, and K. Bechgard, J. Phys. Soc. Jpn. **59**, 2036 (1990).
[101]H. I. Keda, Y. Endoh, and S. Itoh, Phys. Rev. Lett. **64**, 1266 (1990).
[102]P. Debye, H. R. Anderson, Jr., and H. Brumberger, J. Appl. Phys. **28**, 679 (1957).
[103]S. Hendrichs and E. Teller, J. Chem. Phys. **10**, 147 (1942).
[104]K. Torii, T. Tamaki, and N. Wakabayashi, J. Phys. Soc. Jpn. **59**, 3620 (1990).
[105]R. F. Shannon, Jr., C. R. Harkless, and S. E. Nagler, Phys. Rev. B **38**, 9327 (1988).
[106]H. Dosch *et al.*, Phys. Rev. Lett. **60**, 2382 (1988).
[107]X-M. Zha *et al.*, Phys. Rev. Lett. **65**, 2692 (1990).
[108]E. G. McRae, T. M. Buck, R. A. Malic, W. E. Wallace, and J. M. Sanchez, Surf. Sci. **238**, L481 (1990).
[109]N. Wakabayashi (private communication).
[110]N. Wakabayashi, Phys. Rev. B **33**, 6441 (1986).
[111]W. H. Press, B. P. Flannery, S. A. Tenkolsky, and W. T. Vetterling, in *Numerical Recipes in Fortran: The Art of Scientific Computing,* (Cambridge University Press, New York, 1985).

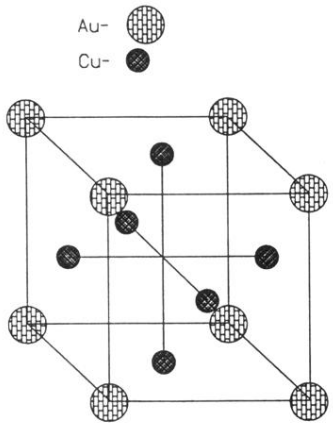

FIG. 2. Schematic of fcc structure for ordered Cu_3Au.